Volume 3 | Number 9 | September 2019

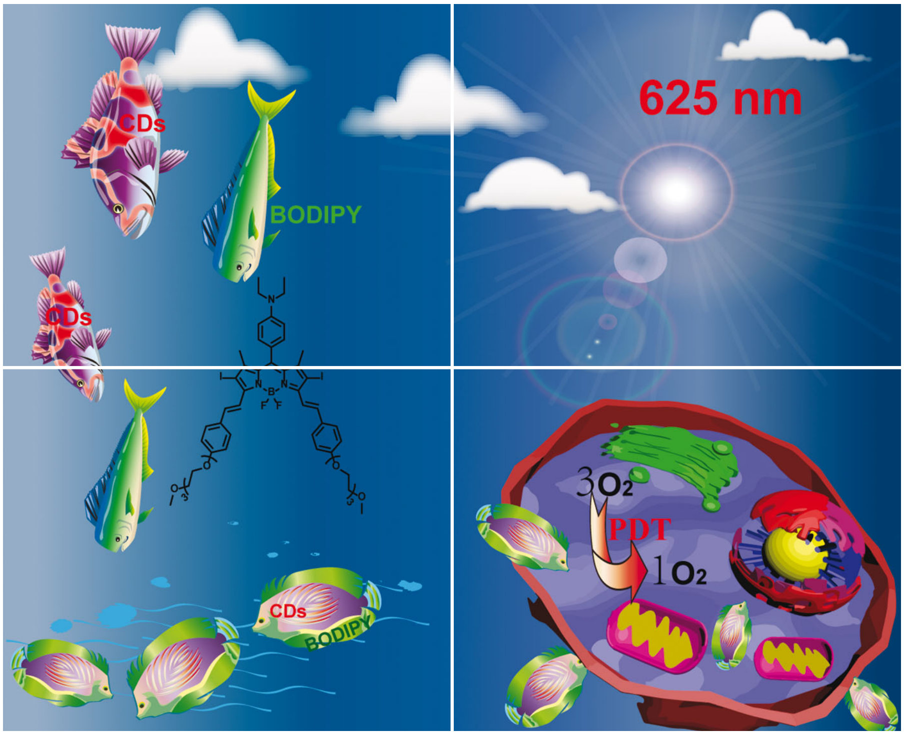

MATERIALS CHEMISTRY FRONTIERS

CCS 中国化学会 CHINESE CHEMICAL SOCIETY
ICCAS
ROYAL SOCIETY OF CHEMISTRY | Celebrating IYPT 2019
rsc.li/frontiers-materials

MATERIALS CHEMISTRY
FRONTIERS

RESEARCH ARTICLE

View Article Online
View Journal | View Issue

Cite this: *Mater. Chem. Front.*, 2019, **3**, 1747

BODIPY@carbon dot nanocomposites for enhanced photodynamic activity†

Ya Su,[a] Siyu Lu,[b] Pengli Gao,[a] Min Zheng*[a] and Zhigang Xie*[c]

Received 23rd April 2019,
Accepted 24th May 2019

DOI: 10.1039/c9qm00257j

rsc.li/frontiers-materials

One stumbling block for the biomedical applications of BODIPY is its poor water solubility. Herein, a type of nanocomposite named CBNPs was fabricated *via* the noncovalent interactions between carbon dots (CDs) and BODIPY, in which the solubility of BODIPY was improved significantly, followed by enhanced photodynamic therapy (PDT) effects through a fluorescence resonance energy transfer (FRET) mechanism. This work provides a conventional strategy to improve the bioavailability of hydrophobic functional materials and demonstrates the great potential of CD-based hybrids in biomedical fields.

Introduction

As a minimally invasive treatment, photodynamic therapy (PDT) exhibits lots of advantages over other traditional treatments (surgery, radiotherapy and chemotherapy), such as low drug resistance, less damage to marginal tissues and fewer side effects.[1–3] As one of the essential factors, photosensitizers (PSs) play an important part in PDT, and can produce cytotoxic reactive oxygen species (ROS) to destroy tumor cells under the irradiation of light.[4–7] To date, various PSs have been developed for PDT, such as boron dipyrromethene (BODIPY), cyanine dyes, porphyrin, chlorin and phthalocyanine derivatives;[8–10] in addition, some scientists have developed self-assembled dye-based nanomaterials for PDT.[11–13] Among these, BODIPY dyes have been used in PDT due to their merits including easy modification, predominant photostability, and high fluorescence quantum yield and molar extinction coefficients.[14–18] However, the intrinsic drawbacks of BODIPY dyes must be addressed, including low water solubility and poor membrane permeability.[19,20] Therefore, developing a conventional strategy to improve the bioavailability of BODIPY and increase the PDT efficacy has become a task of top priority.

Carbon dots (CDs) are a new type of carbon-based luminescent materials, which have a wide range of applications in sensors, bioimaging and drug delivery,[19–25] owing to their advantages of high water solubility, excellent optical properties, good biocompatibility, low toxicity, simple synthesis and easy surface modification.[26–31] In particular, CDs can act as promising carriers by conjugation or co-assembly with drugs, functional dyes or proteins. Our previous work has demonstrated that a CD-based theranostic nanomedicine was successfully constructed by means of covalent binding to oxaliplatin.[26] On the other hand, a CD–doxorubicin hybrid was formed *via* supramolecular interactions.[32] Moreover, we reported the co-assembly of CDs with an AIEgen to achieve the function of long-term biological imaging[20] and combination of CDs and subunit B of ricin toxin to enhance the immunomodulatory activity.[28,33] Inspired by our recent work on CD-based supramolecular hybrids as mentioned above, we anticipated that CDs could also assemble with hydrophobic BODIPY to form fluorescent nanoparticles (NPs) and render BODIPY dispersible in aqueous media. Therefore, in this work, CD–BODIPY NPs (named as CBNPs, Scheme 1) with high dispersibility and stability were prepared by the co-assembly of CDs and BODIPY. The formed CBNPs not only improved the water solubility of BODIPY but also enhanced the PDT efficiency by way of fluorescence resonance energy transfer (FRET), with the CDs as a donor and BODIPY as an acceptor chromophore.

Results and discussion

Preparation and Characterization of CBNPs

The synthesis of BODIPY is based on previous work.[34] Detailed synthesis and characterization of BODIPY can be found in the ESI† (Fig. S1). The CDs were prepared from dopamine and *o*-phenylenediamine.[35] A mixture of CDs and BODIPY (weight ratio, 1 : 1) in *N*,*N*-dimethylformamide (DMF) was slowly added into water and stirred overnight. Then the unassembled CDs and BODIPY were removed by centrifugation at the speed of 5000 rpm for 5 min. The obtained supernatant was dialyzed against deionized water for 24 h. As a contrast, we tried to

[a] *School of Chemistry and Life Science, Advanced Institute of Materials Science, Changchun University of Technology, 2055 Yanan Street, Changchun, Jilin 130012, P. R. China. E-mail: zhengm@ciac.ac.cn*
[b] *College of Materials Science and Engineering, College of Chemistry and Molecular Engineering, Zhengzhou University, Zhengzhou, 450000, P. R. China*
[c] *State Key Laboratory of Polymer Physics and Chemistry, Changchun Institute of Applied Chemistry, Chinese Academy of Sciences, 5625 Renmin Street, Changchun, Jilin 130022, P. R. China. E-mail: xiez@ciac.ac.cn*

† Electronic supplementary information (ESI) available. See DOI: 10.1039/c9qm00257j

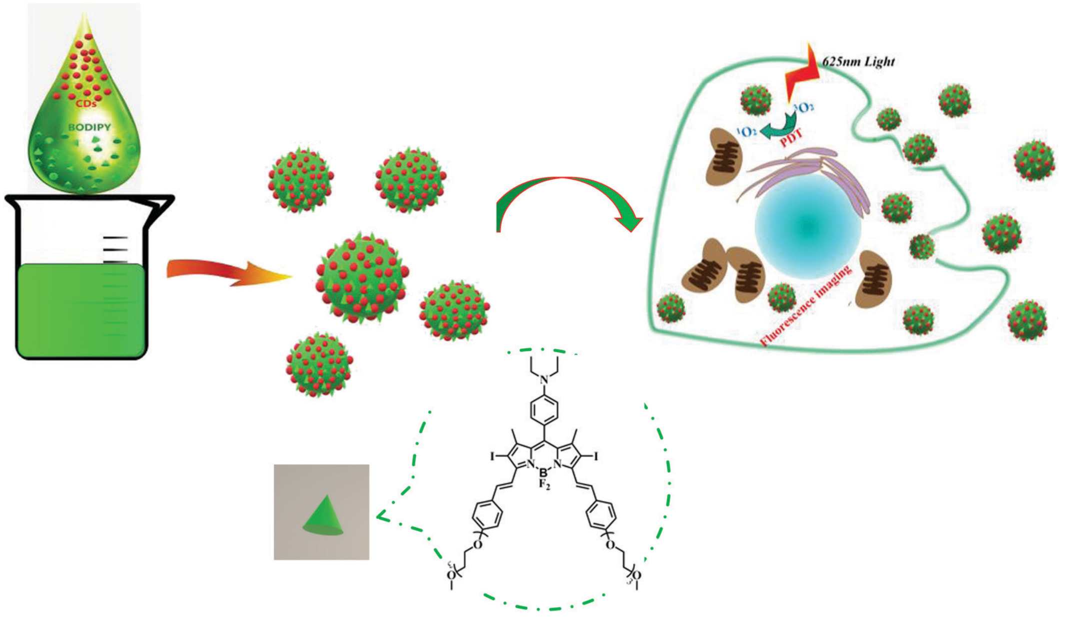

Scheme 1 Schematic illustration of the CBNPs for photodynamic therapy and imaging.

prepare NPs by dropping the DMF solution of BODIPY into water, which is similar to the procedure of synthesizing CBNPs; unfortunately, no NPs were formed. Alternatively, BODIPY NPs (named as BNPs) were constructed by adding a mixture of BODIPY and pluronic F-127 into water and stirring overnight. The morphologies and size distributions of the CDs, CBNPs and BNPs were characterized by transmission electron microscopy (TEM). Fig. 1c reveals the uniform size (3.38 nm) of the CDs, while the monodispersed CBNPs possess the average size of 160.01 nm (Fig. 1a). The average size of the CBNPs determined by dynamic light scattering (DLS) is 150.26 nm (Fig. 1a, the inset), which is consistent with the TEM data. BNPs have an average diameter of 171.85 nm (Fig. 1d). In addition, the absolute fluorescence quantum yield of BODIPY is 23.9%. The absolute fluorescence quantum yield of the CBNPs was 0.6% under the same BODIPY concentration. In summary, the above data means the successful assembly of CDs and BODIPY. The loading efficiency of BODIPY in CBNPs is determined to be

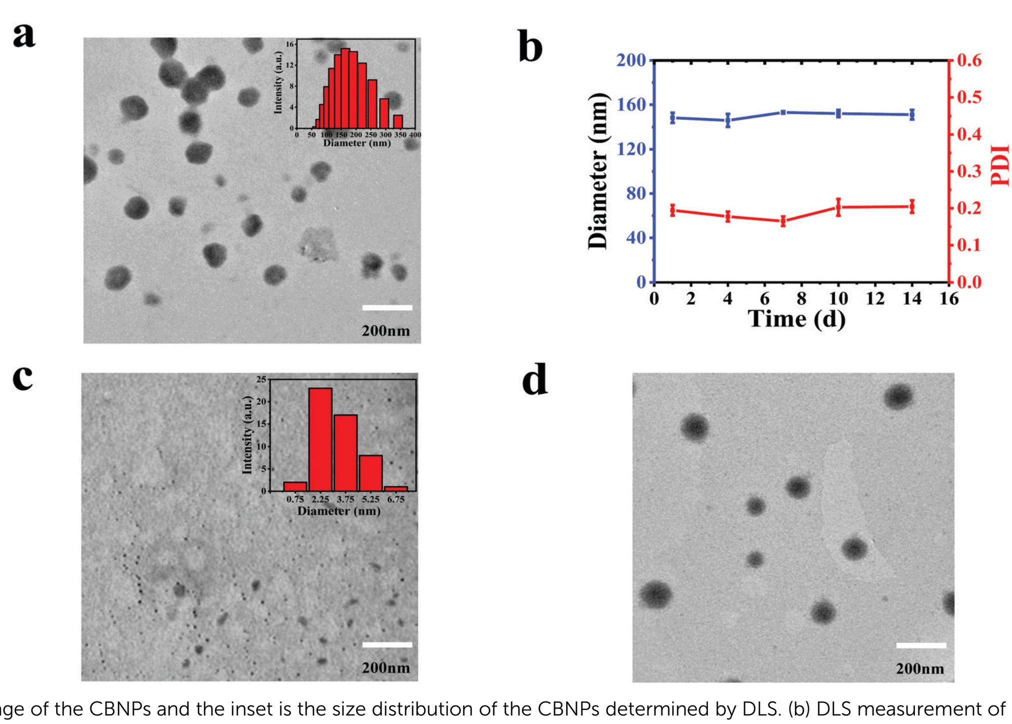

Fig. 1 (a) TEM image of the CBNPs and the inset is the size distribution of the CBNPs determined by DLS. (b) DLS measurement of the CBNPs in water. (c) TEM image of the CDs and the inset is the size distribution of the CDs. (d) TEM image of BNPs.

71.25% according to the BODIPY standard curve (Fig. S2, ESI†). At the same time, in order to verify the stability of the CBNPs in an aqueous solution, we monitored their size changes by DLS.[36] As shown in Fig. 1b, the changes in size of the CBNPs are negligible, and the PDI values of the CBNPs are always less than 0.2, which illustrates that the CBNPs are stable in aqueous solution.

The UV-Vis spectrum of the CDs is displayed in Fig. S3a (ESI†), which has three typical absorption bands at 280, 570 and 611 nm. The photoluminescence (PL) spectra of the CDs (Fig. S3b, ESI†) are conducted under the excitation of 440–600 nm, and the maximum emission peak is at 650 nm under 600 nm irradiation (Fig. 2a, blue solid line). As for BODIPY, it has a maximum absorption band centered at 650 nm (Fig. 2a, red solid line), which overlaps well with the PL spectrum of the CDs, satisfying the pre-requisite of the fluorescence resonance energy transfer (FRET) conditions. Therefore, CDs and BODIPY can act as a donor and an acceptor, respectively, leading to the occurrence of FRET from CDs to BODIPY.[37] In order to study the interaction between CDs and BODIPY, absorption (Fig. 2b) and fluorescence (Fig. 2c) titration experiments were carried out. As shown in Fig. 2b, the absorption intensities of BODIPY reduced gradually on increasing the concentration of CDs. On the other hand, the fluorescence intensities of BODIPY were enhanced on increasing the concentrations of CDs, verifying that the CDs had transferred energy to BODIPY through FRET. It can be seen from Fig. 2d that the CBNPs exhibited two emission bands which are centered at 635 nm and 695 nm, respectively. The intensity ratio of the emission peak of the CDs at 650 nm to the emission peak at 701 nm is 2.9 (Fig. 2d, black solid line). While, for the CBNPs, the intensity ratio of the two corresponding emission peaks is 1.5 (Fig. 2d, green solid line) and one emission peak at 710 nm is observed in BNPs (Fig. 2d, red solid line). Based on the above results, we can conclude that the hybridization of BODIPY with CDs increases the fluorescence intensity of BODIPY at around 710 nm with a simultaneous decrease in the fluorescence intensity of the CDs at around 650 nm. These results irrefutably prove that the FRET effect exists in this hybrid where the CDs work as a donor while BODIPY works as an acceptor.[38–41]

Evaluation of the PDT effects

The ability of the CDs, BNPs, and CBNPs to produce singlet oxygen (SO) was determined by using indocyanine green (ICG) as a probe under the irradiation of a laser (625 nm, 16 mW cm^{-2}), and the absorbance of ICG was further monitored by UV-vis absorption spectra. No obvious changes in the ICG absorbance in the absence (Fig. 3a) and presence of CDs (Fig. 3b) were observed, verifying that CDs have no PDT effect. On the contrary, the absorption intensity of ICG decreased dramatically in the presence of the BNPs (Fig. 3c) or CBNPs (Fig. 3d) upon irradiation, indicating that both BNPs and CBNPs have a high PDT effect. The degradation rate of the CBNPs is as high as 40% after irradiation for 100 s (Fig. 3e), which is higher than that of the BNPs (33%) and CDs (11%), confirming that the CBNPs possess higher ability to generate SO than the BNPs under the same conditions.

In vitro cellular uptake

Intracellular uptake of the CBNPs was investigated by confocal laser scanning microscope (CLSM). Human cervical carcinoma (HeLa) cells were incubated with different concentrations

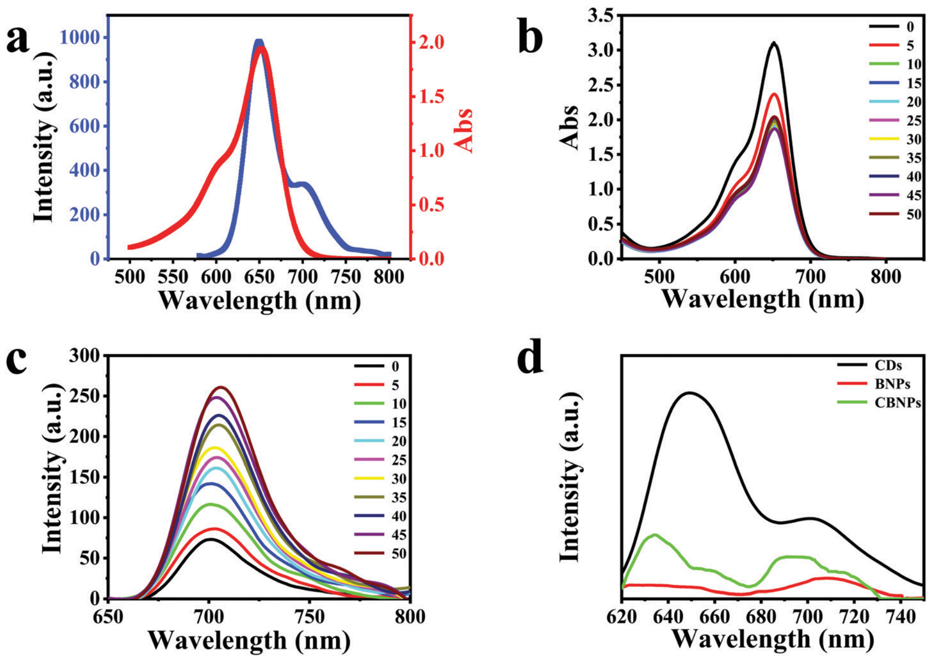

Fig. 2 (a) UV-Vis absorption spectrum of BODIPY (red solid line) and the PL spectrum (blue solid line) of CDs under 560 nm excitation in aqueous solution; (b) UV-Vis spectra of BODIPY (50 μg mL^{-1}) with increasing concentration of CDs from 0 to 50 μg mL^{-1}. (c) PL spectra of BODIPY (50 μg mL^{-1}) excited at 600 nm during the titration of CDs (0–50 μg mL^{-1}) at room temperature. (d) PL spectra of CDs, BNPs, and CBNPs (excitation at 580 nm).

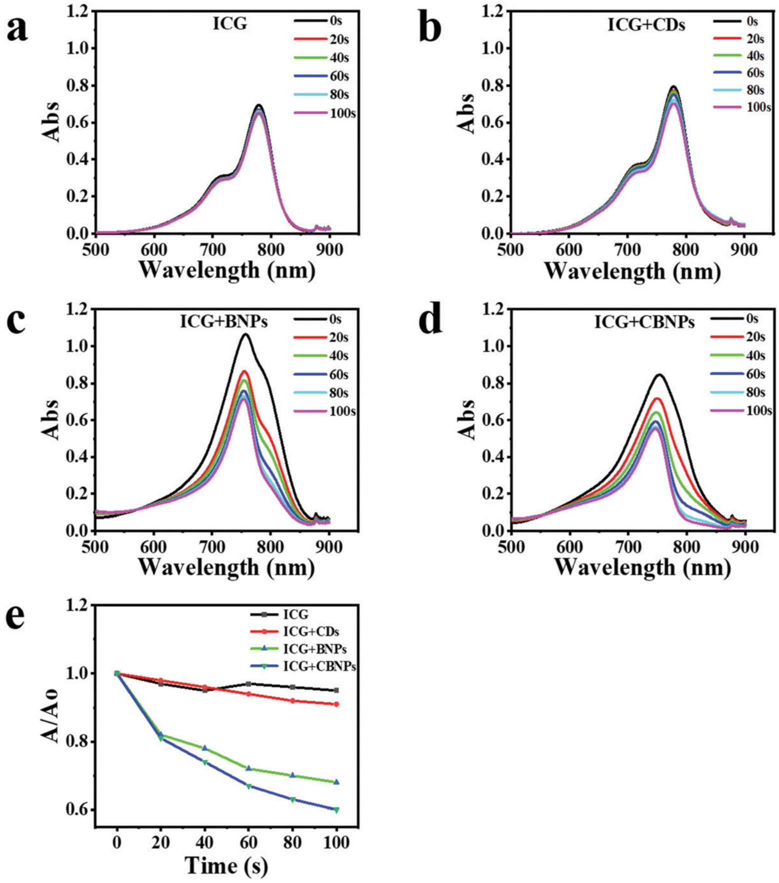

Fig. 3 Assessment of singlet oxygen generation ability. The absorption changes of (a) ICG, (b) ICG + CDs (c) ICG + BNPs and (d) ICG + CBNPs upon 625 nm irradiation (16 mW cm^{-2}). (e) The degradation rate of ICG (black), ICG + CDs (red), ICG + BNPs (green).

(1, 2 and 4 μg mL^{-1}) of the CBNPs for 6 h at 37 °C.[5,42,43] As displayed in Fig. 4a, the fluorescence intensities of HeLa cells were enhanced gradually as the concentration of the CBNPs increased, confirming the concentration-dependent endocytosis. When HeLa cells were incubated with the CBNPs (1 μg mL^{-1}) for 0.5, 2, and 6 h at 37 °C, the fluorescence intensities of the HeLa cells increased with prolonged incubation time (Fig. 4b), indicating that HeLa cells can effectively internalize CBNPs in a time-dependent manner. Moreover, in order to further quantify the endocytosis, flow cytometry was carried out.[44–46] According to the results of flow cytometry analysis (Fig. 4c), the endocytosis for red fluorescence intensity was gradually enhanced with prolonged incubation time, consistent with the above CLSM images. In order to further prove the changes in fluorescence intensity of CLSM, we quantified the fluorescence intensity of CLSM with the ImageJ software. As shown in Fig. 4d, the red fluorescence intensity really increased with time.

In vitro PDT effects of CBNPs

The *in vitro* cytotoxicity of the CBNPs against HeLa cells was determined by the standard thiazolyl blue tetrazolium bromide (MTT) assay. As shown in Fig. 5a, the cell viabilities of HeLa cells in the CD, BNP and CBNP groups are 95.9%, 97.6% and 102%, respectively, which verifies that the CDs, BNPs and CBNPs

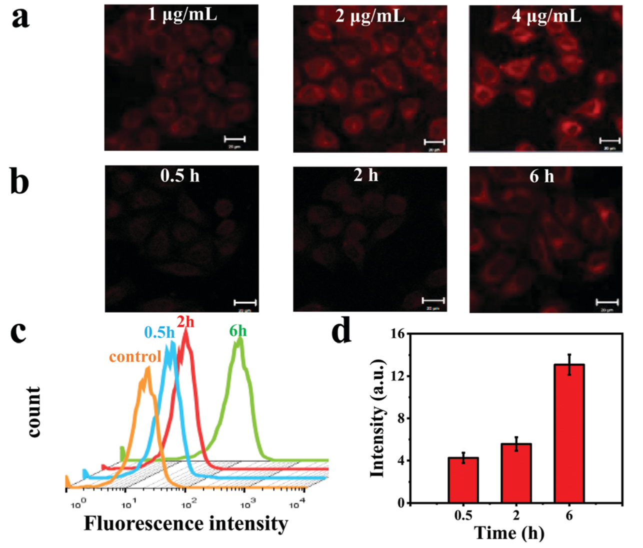

Fig. 4 The representative CLSM images of HeLa cells incubated with CBNPs (a) at the concentrations of 0.5, 1, 2, 4 μg mL^{-1}, respectively for 6 h. (b) CBNPs (1 μg mL^{-1}) for 0.5, 2 and 6 h. For each panel, scale bar, 20 μm. (c) Flow cytometry analysis of cellular uptake of the CBNPs in HeLa cells at 0.5, 2 and 6 h. (d) Quantitative analysis of the red fluorescence intensity of the CLSM with ImageJ software.

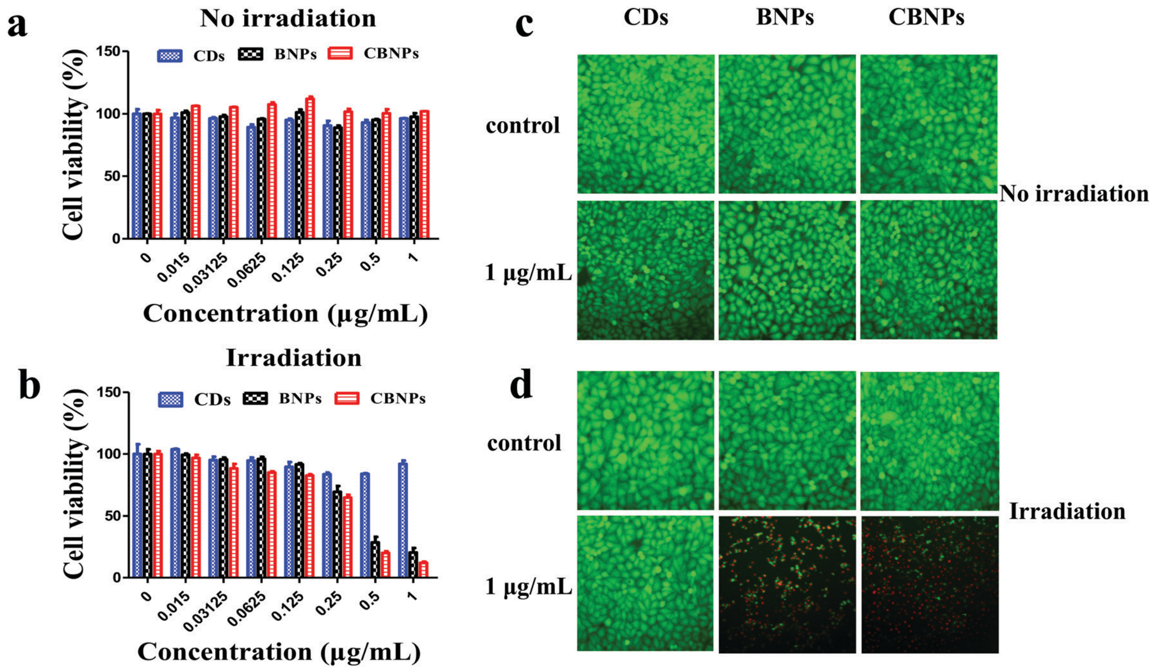

Fig. 5 Cell cytotoxicities of the CDs, BNPs, and CBNPs without (a) or with (b) irradiation (625 nm laser, 16 mW cm^{-2}) for 30 min against HeLa cells after incubation for 48 h. The fluorescence microscopic images of HeLa cells co-stained with calcein AM (green, live cells) and propidium iodide (red, dead cells) after being incubated with 1 μg mL^{-1} of the CDs, BNPs, and CBNPs without (c) or with (d) irradiation.

have no apparent toxicity toward HeLa cells in the absence of irradiation. Then we studied the phototoxicities of CDs, BNPs and CBNPs under the irradiation of a 625 nm laser (16 mW cm^{-2}) for 30 min. As shown in Fig. 5b, the cell survival rate for the group of CDs is 91.9%, indicating that CDs have no obvious phototoxicity. In contrast, the cell survival rate for the BNPs and CBNPs is 19.55% and 10.8%, respectively. These results further confirm that the CBNPs exhibit a higher PDT effect than the BNPs. In addition, in order to intuitively study the PDT efficiency of CBNPs, a live/dead staining experiment was used to verify the apoptosis and necrosis of cells under irradiation. After incubation with 1 μg mL^{-1} of the CDs, BNPs, CBNPs, respectively, HeLa cells were stained with the fluorescent probes calcein AM (live cells) and propidium iodide (PI, dead cells). As shown in Fig. 5c, intense green fluorescence is observed for the three groups, indicating that the CDs, BNPs and CBNPs had good cytocompatibility. As for CDs, no dead cells are detected even under laser irradiation (Fig. 5d), certifying that CDs have no phototoxicity. Meanwhile, strong red and weak green fluorescence was found for the groups of BNPs and CBNPs (Fig. 5d); moreover, the amount of dead cells in the CBNP group is higher than that in the BNP group, manifesting that CBNPs possess more effective PDT than BNPs. These results are consistent with the MTT assay.

Dual fluorescence of Annexin V-FITC/PI was measured by flow cytometry to detect the apoptosis of cells at different stages.[4,47] As shown in Fig. 6, without irradiation, the cell viability of the CDs, BNPs and CBNPs is comparable to that of the control group, which indicated that all the groups had no cytotoxicity without irradiation. However, under continuous irradiation of a 625 nm laser (16 mW cm^{-2}) for 30 min, the percentage of dead and apoptotic cells is 98.62% and 66.22% for the CBNP group, respectively. Under the same concentration, the percentage of dead cells in the BNP group is 76.69%, which further confirms that the CBNPs have higher phototoxic effects than the BNPs. Therefore, the co-assembly of CDs with BODIPY improved the PDT efficiency of the CBNPs.

Experimental

Preparation of CBNPs

Typically, CDs (500 μg) and BODIPY (500 μg) are dissolved in *N*,*N*-dimethylformamide (DMF) with a volume of 3 mL; thereafter, the mixed solution was slowly added into water (10 mL) and stirred for overnight. Then the unassembled CDs and BODIPY were removed by centrifugation (5000 rpm) for 5 minutes. The obtained supernatant was placed in a dialysis bag (M_w cutoff: 3.5 kDa) and dialyzed against deionized water for 24 h. Finally, CBNPs were obtained.

Preparation of BNPs

BODIPY (500 μg) and F-127 (500 μg) were mixed together in DMF solution (3 mL); then, the mixture was slowly added into deionized water (10 mL). After that, the mixture was stirred overnight, and the unassembled BODIPY and F-127 were removed by centrifugation (the speed is 5000 rpm) for 5 minutes. The obtained supernatant was placed in a dialysis bag (M_w cutoff: 3.5 kDa) and dialyzed against deionized water for 24 h. Finally, BNPs were obtained.

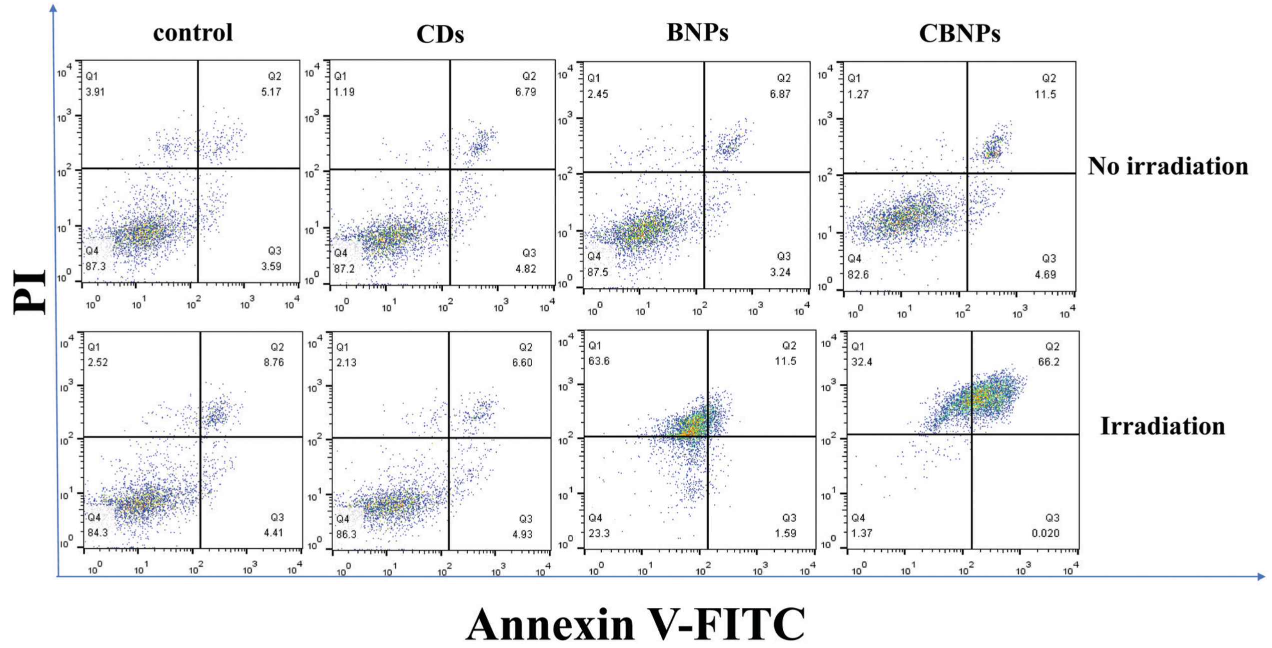

Fig. 6 Flow cytometry analysis of early and late apoptosis of HeLa cells incubated with PBS (control), CDs, BNPs and CBNPs for 24 h at the concentration of 1 μg mL^{-1}, and then treated with or without light irradiation. The four quadrants indicated the four statuses of cells: necrotic (Q1), late-stage apoptotic (Q2), early apoptotic (Q3), and live (Q4).

Conclusions

In summary, we developed a straightforward strategy to fabricate a kind of nanocomposite named CBNPs *via* the coassembly of CDs and BODIPY, by which the solubility and PDT effects of BODIPY were significantly improved through the FRET mechanism. The CBNPs exhibit good water solubility, excellent $^1O_2$ quantum yield, and high biocompatibility and PDT efficiency. We believe that this supermolecular coassembly approach may open up a new way of formulating multifunctional hybrids and expanding their potential applications in biomedical fields and cancer treatment.

Conflicts of interest

There are no conflicts to declare.

Acknowledgements

The financial support from the National Natural Science Foundation of China (No. 51873023 and 51522307) is gratefully acknowledged.

Notes and references

1 X. Li, S. Lee and J. Yoon, *Chem. Soc. Rev.*, 2018, **47**, 1174–1188.
2 Y. Liu, N. Song, L. Chen, S. Liu and Z. Xie, *Chem. – Asian J.*, 2018, **13**, 989–995.
3 P. Agostinis, K. Berg, K. A. Cengel, T. H. Foster, A. W. Girotti, S. O. Gollnick, S. M. Hahn, M. R. Hamblin, A. Juzeniene, D. Kessel, M. Korbelik, J. Moan, P. Mroz, D. Nowis, J. Piette, B. C. Wilson and J. Golab, *Ca-Cancer J. Clin.*, 2011, **61**, 250–281.
4 X. Zheng, L. Wang, M. Liu, P. Lei, F. Liu and Z. Xie, *Chem. Mater.*, 2018, **30**, 6867–6876.
5 X. Zheng, L. Wang, Q. Pei, S. He, S. Liu and Z. Xie, *Chem. Mater.*, 2017, **29**, 2374–2381.
6 S. S. Lucky, K. C. Soo and Y. Zhang, *Chem. Rev.*, 2015, **115**, 1990–2042.
7 Y. Cai, P. Liang, Q. Tang, X. Yang, W. Si, W. Huang, Q. Zhang and X. Dong, *ACS Nano*, 2017, **11**, 1054–1063.
8 J. He, Y. Wang, M. A. Missinato, E. Onuoha, L. A. Perkins, S. C. Watkins, C. M. St Croix, M. Tsang and M. P. Bruchez, *Nat. Methods*, 2016, **13**, 263.
9 X. Liu, M. Wu, Q. Hu, H. Bai, S. Zhang, Y. Shen, G. Tang and Y. Ping, *ACS Nano*, 2016, **10**, 11385–11396.
10 Y. Cai, W. Si, Q. Tang, P. Liang, C. Zhang, P. Chen, Q. Zhang, W. Huang and X. Dong, *Nano Res.*, 2017, **10**, 794–801.
11 S. Li, Q. Zou, Y. Li, C. Yuan, R. Xing and X. Yan, *J. Am. Chem. Soc.*, 2018, **140**, 10794–10802.
12 M. Abbas, Q. Zou, S. Li and X. Yan, *Adv. Mater.*, 2017, 29.
13 K. Liu, R. Xing, Q. Zou, G. Ma, H. Mohwald and X. Yan, *Angew. Chem., Int. Ed.*, 2016, **55**, 3036–3039.
14 N. Mukherjee, S. Podder, K. Mitra, S. Majumdar, D. Nandi and A. R. Chakravarty, *Dalton Trans.*, 2018, **47**, 823–835.
15 N. Boens, V. Leen and W. Dehaen, *Chem. Soc. Rev.*, 2012, **41**, 1130–1172.
16 S. Kolemen and E. U. Akkaya, *Coord. Chem. Rev.*, 2018, **354**, 121–134.
17 T. Sun, X. Guan, M. Zheng, X. Jing and Z. Xie, *ACS Med. Chem. Lett.*, 2015, **6**, 430–433.
18 J. Y. Liu, P. Z. Zhou, J. L. Ma and X. Jia, *Molecules*, 2018, 23.
19 X. Dai, X. Chen, Y. Zhao, Y. Yu, X. Wei, X. Zhang and C. Li, *Biomacromolecules*, 2018, **19**, 141–149.

20 J. Zou, Z. Yin, K. Ding, Q. Tang, J. Li, W. Si, J. Shao, Q. Zhang, W. Huang and X. Dong, *ACS Appl. Mater. Interfaces*, 2017, **9**, 32475–32481.
21 X. Miao, X. Yan, D. Qu, D. Li, F. F. Tao and Z. Sun, *ACS Appl. Mater. Interfaces*, 2017, **9**, 18549–18556.
22 J. A. Jaleel and K. Pramod, *J. Controlled Release*, 2018, **269**, 302–321.
23 J. Zhang, M. Zheng, F. Zhang, B. Xu, W. Tian and Z. Xie, *Chem. Mater.*, 2016, **28**, 8825–8833.
24 T. Feng, X. Ai, G. An, P. Yang and Y. Zhao, *ACS Nano*, 2016, **10**, 4410–4420.
25 A. Mewada, S. Pandey, M. Thakur, D. Jadhav and M. Sharon, *J. Mater. Chem. B*, 2014, **2**, 698–705.
26 M. Zheng, S. Liu, J. Li, D. Qu, H. Zhao, X. Guan, X. Hu, Z. Xie, X. Jing and Z. Sun, *Adv. Mater.*, 2014, **26**, 3554–3560.
27 H. Wang, S. Mukherjee, J. Yi, P. Banerjee, Q. Chen and S. Zhou, *ACS Appl. Mater. Interfaces*, 2017, **9**, 18639–18649.
28 Y. Li, W. Liu, C. Sun, M. Zheng, J. Zhang, B. Liu, Y. Wang, Z. Xie and N. Xu, *J. Colloid Interface Sci.*, 2018, **523**, 226–233.
29 D. Li, D. Wang, X. Zhao, W. Xi, A. Zebibula, N. Alifu, J.-F. Chen and J. Qian, *Mater. Chem. Front.*, 2018, **2**, 1343–1350.
30 H. Singh, J. S. Sidhu, D. K. Mahajan and N. Singh, *Mater. Chem. Front.*, 2019, **3**, 476–483.
31 Y.-Y. Huang, Y. Tian, X.-Q. Liu, Z. Niu, Q.-Z. Yang, V. Ramamurthy, C.-H. Tung, Y.-Z. Chen and L.-Z. Wu, *Mater. Chem. Front.*, 2018, **2**, 1893–1899.
32 T. Sun, M. Zheng, Z. Xie and X. Jing, *Mater. Chem. Front*, 2017, **1**, 354–360.
33 J. Zhang, M. Zheng and Z. Xie, *J. Mater. Chem. B*, 2016, **4**, 5659–5663.
34 N. Song, L. Fu, Y. Liu, Y. Li, L. Chen, X. Wang, S. Liu and Z. Xie, *Dyes Pigm.*, 2019, **162**, 295–302.
35 S. Lu, L. Sui, J. Liu, S. Zhu, A. Chen, M. Jin and B. Yang, *Adv. Mater.*, 2017, 29.
36 J. Zhang, L. Wang and Z. Xie, *ACS Biomater. Sci. Eng.*, 2017, **4**, 1969–1975.
37 K. Yang, F. Li, W. Che, X. Hu, C. Liu and F. Tian, *RSC Adv.*, 2016, **6**, 101447–101451.
38 T. Chiaki, H. Dailo, O. Issey and K. Hideya, *Acta Physiol.*, 2018, 805–811.
39 J. Qiu, S. Jiang, H. Guo and F. Yang, *Dyes Pigm.*, 2018, **157**, 351–358.
40 J. Shao, H. Sun, H. Guo, S. Ji, J. Zhao, W. Wu, X. Yuan, C. Zhang and T. D. James, *Chem. Sci.*, 2012, **3**, 1049–1061.
41 D. Su, C. L. Teoh, S. Sahu, R. K. Das and Y. T. Chang, *Biomaterials*, 2014, **35**, 6078–6085.
42 H. He, X. Zheng, S. Liu, M. Zheng, Z. Xie, Y. Wang, M. Yu and X. Shuai, *Nanoscale*, 2018, **10**, 10991–10998.
43 Q. Pei, X. Hu, X. Zheng, S. Liu, Y. Li, X. Jing and Z. Xie, *ACS Nano*, 2018, **12**, 1630–1641.
44 Y. Liu, N. Song, L. Chen and Z.-G. Xie, *Chin. J. Polym. Sci.*, 2017, **36**, 417–424.
45 Y. Li, N. Xu, W. Zhu, L. Wang, B. Liu, J. Zhang, Z. Xie and W. Liu, *ACS Appl. Mater. Interfaces*, 2018, **10**, 22974–22984.
46 V. Ramu, S. Gautam, A. Garai, P. Kondaiah and A. R. Chakravarty, *Inorg. Chem.*, 2018, **57**, 1717–1726.
47 X. Zheng, L. Wang, S. Liu, W. Zhang, F. Liu and Z. Xie, *Adv. Funct. Mater.*, 2018, **28**, 1706507.